THE JOURNAL OF BIOLOGICAL CHEMISTRY VOL. 285, NO. 47, pp. 36608–36615, November 19, 2010

Structural and Kinetic Characterization of 4-Hydroxy-4-methyl-2-oxoglutarate/4-Carboxy-4-hydroxy-2-oxoadipate Aldolase, a Protocatechuate Degradation Enzyme Evolutionarily Convergent with the HpaI and DmpG Pyruvate Aldolases*[S]

Received for publication, June 29, 2010, and in revised form, September 3, 2010 Published, JBC Papers in Press, September 15, 2010, DOI 10.1074/jbc.M110.159509

Weijun Wang, Scott Mazurkewich, Matthew S. Kimber[1], and Stephen Y. K. Seah[2]

From the Department of Molecular and Cellular Biology, University of Guelph, Guelph, Ontario N1G 2W1, Canada

4-Hydroxy-4-methyl-2-oxoglutarate/4-carboxy-4-hydroxy-2-oxoadipate (HMG/CHA) aldolase from *Pseudomonas putida* F1 catalyzes the last step of the bacterial protocatechuate 4,5-cleavage pathway. The preferred substrates of the enzyme are 2-keto-4-hydroxy acids with a 4-carboxylate substitution. The enzyme also exhibits oxaloacetate decarboxylation and pyruvate α-proton exchange activity. Sodium oxalate is a competitive inhibitor of the aldolase reaction. The pH dependence of k_{cat}/K_m and k_{cat} for the enzyme is consistent with a single deprotonation with pK_a values of 8.0 ± 0.1 and 7.0 ± 0.1 for free enzyme and enzyme substrate complex, respectively. The 1.8 Å x-ray structure shows a four-layered α-β-β-α sandwich structure with the active site at the interface of two adjacent subunits of a hexamer; this fold resembles the RNase E inhibitor, RraA, but is novel for an aldolase. The catalytic site contains a magnesium ion ligated by Asp-124 as well as three water molecules bound by Asp-102 and Glu-199′. A pyruvate molecule binds the magnesium ion through both carboxylate and keto oxygen atoms, completing the octahedral geometry. The carbonyl oxygen also forms hydrogen bonds with the guanadinium group of Arg-123, which site-directed mutagenesis confirms is essential for catalysis. A mechanism for HMG/CHA aldolase is proposed on the basis of the structure, kinetics, and previously established features of other aldolase mechanisms.

Protocatechuate is a key intermediate in the microbial degradation of diverse aromatic compounds, including low molecular weight products derived from lignin degradation, such as vanillate and syringate (1), pollutants from fossil fuels and coal derivatives such as fluorene and its analogs (2), and man-made xenobiotics such as phthalate isomers found in plastics and pesticides (1, 3). The aromatic ring cleavage of protocatechuate in the microbial 4,5-cleavage pathway leads to formation of 4-carboxy-2-hydroxymuconate-6-semialdehyde. Depending on the bacteria strain, this intermediate can be converted to 4-hydroxy-4-methyl-2-oxoglutarate (HMG)[3] in the hydrolytic branch of the pathway or 4-carboxy-4-hydroxy-2-oxoadipate (CHA) in the oxidative branch (4). Carbon-carbon bond cleavage catalyzed by a common aldolase (HMG/CHA aldolase; EC 4.1.3.17) leads to formation of two molecules of pyruvate in the former case and a molecule of pyruvate and oxaloacetate in the latter (Fig. 1), which can then be channeled to the TCA cycle (5).

Aldolases are an evolutionarily diverse class of enzymes that are typically divided into two groups based on their catalytic mechanism. The Class I aldolases utilize a Schiff base mechanism to stabilize a carbanion intermediate, whereas the Class II enzymes utilize divalent metal ions to stabilize an enolate intermediate. Within each mechanistic class of aldolases, further diversity exists with respect to the sequence, structure, and substrate specificities. HMG/CHA aldolases have previously been purified from *Pseudomonas putida* and *Pseudomonas ochraceae* and found to be divalent metal ion-dependent Class II aldolases (5, 6). However, the amino acid sequence of the *P. orchraceae* enzyme (7) showed no sequence similarity to other well studied Class II pyruvate aldolases, including HpaI (8) and DmpG (9) from the bacterial degradation pathways of 4-hydroxyphenylacetate and phenol, respectively. Therefore, HMG/CHA aldolases have been proposed to be distinct members of Class II pyruvate aldolases in aromatic degradation pathways (COG0684 for HMG/CHA aldolases, COG3836 for HpaI, and COG0119 for DmpG). Intriguingly, the HMG/CHA aldolases are distantly related in sequence to RraA (regulator of ribonuclease activity A) proteins (sequence identities of 25–33% over the central ~115 residues and ~15% over entire sequence), which associate within the RNA degradosome and inhibit RNase E activity in *Escherichia coli* (10), and a yeast

* This work was supported by National Science and Engineering Research Council of Canada Discovery Grants 238284 (to S. Y. K. S.) and 327280 (to M. S. K.).

[S] The on-line version of this article (available at http://www.jbc.org) contains supplemental Tables S1 and S2 and Figs. S1–S5.

The atomic coordinates and structure factors (code 3NOJ) have been deposited in the Protein Data Bank, Research Collaboratory for Structural Bioinformatics, Rutgers University, New Brunswick, NJ (http://www.rcsb.org/).

[1] To whom correspondence may be addressed: Dept. of Molecular and Cellular Biology, University of Guelph, Guelph, ON N1G 2W1, Canada. Tel.: 519-824-4120; Fax: 519-837-1802; E-mail: mkimber@uoguelph.ca.

[2] To whom correspondence may be addressed: Dept. of Molecular and Cellular Biology, University of Guelph, Guelph, ON N1G 2W1, Canada. Tel.: 519-824-4120; Fax: 519-837-1802; E-mail: sseah@uoguelph.ca.

[3] The abbreviations used are: HMG, 4-hydroxy-4-methyl-2-oxoglutarate or 2-hydroxy-2-methyl-4-oxopentanedioic acid; CHA, 4-carboxy-4-hydroxy-2-oxoadipic acid or 2-hydroxy-4-oxobutane-1,2,4-tricarboxylic; KHG, α-keto-γ-hydroxyglutarate or 2-hydroxy-4-oxopentanedioic acid; HOPA, 4-hydroxy-2-oxopentanoate; LDH, L-lactate dehydrogenase; MDH, malic dehydrogenase; MOPS, 3-(*N*-morpholino) propanesulfonic acid; MES, 2-(*N*-morpholine)ethanesulfonic acid; OAA, oxaloacetate.

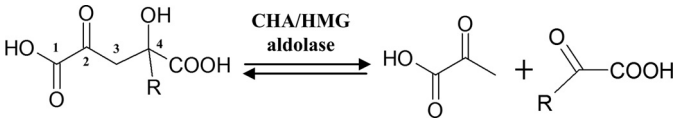

FIGURE 1. **Scheme showing the aldol cleavage reaction catalyzed by HMG/CHA aldolase.** R is CH_3 for HMG and CH_2COOH for CHA.

protein (YER010c) of known structure but unknown function (11).

In addition to their importance in aromatic compounds and carbohydrate metabolism, the ability of aldolases to catalyze the formation of carbon-carbon bond linkages has resulted in them also being exploited as biocatalysts to synthesize natural products and bioactive molecules (12). Here, we kinetically characterize HMG/CHA aldolase from *P. putida* F1 (56% sequence identity to the *P. orchracea* enzyme), show that its structure is characterized by an RraA-like fold previously unseen in aldolases, and find conserved features in common with distantly related and poorly characterized homologs. Our results provide significant new insights into the active site organization and the potential catalytic mechanism of this enzyme, which should facilitate efforts to engineer aldolases to enhance aromatic pollutant degradation and for use as a biocatalyst.

EXPERIMENTAL PROCEDURES

Chemicals—Sodium pyruvate, sodium oxalate, oxaloacetate, L-lactate dehydrogenase (LDH, rabbit muscle), malate dehydrogenase (MDH, porcine heart), and Dowex® 1X8-200 ion exchange resin were from Sigma-Aldrich. Restriction enzymes, T4 DNA ligase, and Pfx polymerase were from Invitrogen or New England Biolabs (Pickering, Canada). All other chemicals were analytical grade and were obtained from Sigma-Aldrich or Fisher.

DNA Manipulation—DNA was purified, digested, and ligated using standard protocols (13). The HMG/CHA aldolase gene (pput1361) was amplified from genomic DNA of *P. putida* F1 by PCR using the primers with the sequences GCGGCATATGAACACTCTGATCGGTAAAAC and CCGCAAGCTTAACCCTCCAAGTCTTCG. Introduced NdeI and PstI restriction sites are underlined. The amplified fragment was ligated to the vector pT7-7 (14). Site-specific mutagenesis was carried out according to a modified QuikChange™ (Stratagene) method. The sequence of the sense oligonucleotides used to construct the R123A and R123K mutants are GGAGTCGCGGACACCCAGACGTTACGCGACATGGGGTTC and GGAGTCAAGGACACCCAGACGTTACGCGACATGGGGTTC, respectively (the altered codons are underlined). All of the constructs were checked by sequencing at the Guelph Molecular Supercenter of the University of Guelph.

Purification of Wild-type and Mutant HMG/CHA Aldolase—Recombinant *E. coli* BL21(λDE3) harboring the gene encoding HMG/CHA aldolase was propagated in 1 liter of Luria-Bertani medium supplemented with 0.6 M D-sorbitol, 2.5 mM glycine betaine, and 100 μg/ml ampicillin at 37 °C until a density of 0.6 was reached at 600-nm wavelength, after which 0.5 mM isopropyl β-D-thiogalactopyranoside was added to induce protein expression. The culture was incubated at 15 °C overnight and then harvested by centrifugation at 5000 × *g* for 10 min.

Chromatography was performed on an ÄKTA Explorer 100 (Amersham Biosciences). Buffer containing 20 mM sodium HEPES, pH 7.5, was used throughout the purification procedure unless indicated otherwise.

The cell pellet (4.1 g of wet weight) was resuspended in buffer and disrupted by a French press. The cell debris was removed by centrifugation (17,500 × *g*, 10 min). The clear supernatant was filtered through a 0.45-μm filter and loaded onto a Source™ 15Q (Amersham Biosciences) anion exchange column (2 × 13 cm). The column was washed with 2 column volumes of the buffer containing 0.15 M NaCl followed by a linear gradient of NaCl from 0.15 to 0.50 M over 12 column volumes. The aldolase was eluted with ~0.35 M NaCl. Active fractions were pooled, concentrated by ultrafiltration with a YM10 filter (Millipore, Nepean, Canada), and loaded onto a phenyl-Sepharose™ hydrophobic interaction chromatography column (1 × 18.5 cm) and purified with a 5-column volume linear gradient of ammonium sulfate from 0.4 to 0 M. The enzyme was eluted at ~0.2 M ammonium sulfate. Active fractions were concentrated to ~4 ml by ultrafiltration, loaded onto a HiLoad 26/60 Superdex 200 prep gel filtration column (Amersham Biosciences), and then eluted with buffer containing 0.15 M NaCl. The purified enzyme was concentrated to 20 mg of protein/ml as before, aliquoted, and stored at −80 °C in 20 mM sodium HEPES buffer, pH 7.5. The enzyme remained stable for 2 months under this storage condition.

Determination of Protein Concentration, Purity, and Molecular Mass—Protein concentrations were determined by the Bradford assay (15) using bovine serum albumin as standards. SDS-PAGE was performed and stained with Coomassie Blue according to established procedures (15). The molecular weight of holoenzyme was determined by gel filtration using a HiLoad 26/60 Superdex 200 prep column.

Crystallization and Structure Determination—HMG/CHA aldolase crystals were grown using the hanging drop method at 25 °C, with 2 μl of reservoir solution containing 10% PEG 4000, 0.2 M ammonium acetate, 0.1 M sodium acetate, pH 4.6, 10 mM $MgCl_2$, 5 mM sodium pyruvate, and 2 μl of 21 mg/ml HMG/CHA aldolase. The crystals were flash frozen in a 100 K liquid nitrogen stream using paratone-N oil as a cryoprotectant. The data were collected to 1.82 Å at the Canadian Macromolecular Crystallography Facility (08ID-1) and processed in HKL2000 (16). Crystals were of the trigonal space group R32, with cell dimensions $a = b = 111.18$ Å and $c = 139.57$ Å. The structure was determined using Phaser (17), searching with residues 2–157 of one protomer from the *Mycobacterium tuberculosis* RraA (MenG) structure (Protein Data Bank code 1NXJ); this solution was weak (LLG 41.4) but proved sufficient for structure refinement. The structure was rebuilt in Coot (18), and refinement was performed using Refmac in CCP4 (19). For the final stages of refinement, TLS refinement with five residue groups was added (20). The crystal contains a single protomer in the asymmetric unit, with residues 1 and 237–238 missing from the final model. Supplemental Table S1 lists data collection and final model refinement statistics. Structure figures were prepared using PyMol (21).

Preparation of Enzyme Substrates—HMG and CHA were synthesized chemically using published methods with some

modifications (22). Racemic KHG and HOPA were synthesized enzymatically using HpaI according to previous methods (23). All of the products were purified using Dowex Chloride 1X8 anion exchange resin with a linear gradient of HCl from 0.0 to 0.1 M. Fractions containing specified products were collected and neutralized by 2.0 M NaOH, lyophilized, and stored at −20 °C. The concentration of each product was determined with HMG/CHA aldolase (using 1.0 mM $CoCl_2$ as cofactor) by coupling pyruvate or oxaloacetate formation to NADH oxidation using LDH or MDH (for CHA), respectively.

Metal Substitution—Metal-free apoenzyme was prepared by adding 0.5 g of Chelex 100 (Sigma) to 10 mg of purified enzyme in 10 ml of 20 mM sodium HEPES, pH 7.5. After gentle stirring for 20 min, Chelex 100 was removed by a 20-μm filter. The apoenzyme has less than 1.0% of the activity observed in the presence of 1.0 mM $MgCl_2$. The apoenzyme was preincubated with the stated metal ions prior to use in the kinetic assay.

Enzyme Assays—All of the kinetics assays were performed at least in duplicate at 25 °C using a Varian Cary 3 spectrophotometer equipped with a thermojacketed cuvette holder. HMG aldol cleavage and OAA decarboxylase activity were observed by coupling pyruvate formation to NADH oxidation using LDH. Analogously, formation of acetaldehyde by HOPA cleavage was monitored using alcohol dehydrogenase, and formation of oxaloacetate by CHA cleavage was monitored using MDH. NADH oxidation was monitored at 340 nm, and the extinction coefficient of NADH was taken to be 6200 M^{-1} cm^{-1}. A standard aldolase cleavage activity assay contained 2.0 mM of substrate, 0.4 mM NADH, 1.0 mM divalent metal ion, and 30 units of either LDH, alcohol dehydrogenase, or MDH in 100 mM HEPES buffer, pH 8.0. For KHG aldol cleavage activity, glyoxylate formation was determined using phenylhydrazine hydrochloride according to the continuous spectrophotometric method (24). Assay solutions contained 4.0 mM phenylhydrazine hydrochloride, 1 mM divalent metal ion, and varying concentrations of KHG in 100 mM HEPES buffer, pH 8.0, with a total volume of 1.0 ml. Enzyme was added to initiate the reaction, and the absorbance increase at 324 nm was monitored for 5 min.

All of the kinetic data fitting was performed using nonlinear regression in the program Leonora (25). All of the data were fitted to the Michaelis-Menten equation, except for the OAA decarboxylation reaction, which was fitted to the substrate inhibition equation. For inhibition assays, the concentration of sodium oxalate was varied from 0.5 to 10 × K_i, and data were fitted to a competitive inhibition equation.

The pH dependence of the kinetics was determined using HMG as the substrate, with pH varying between pH 6.0 and 10.5 in a three-component constant ionic strength buffer containing 0.1 M Tris, 0.05 M acetic acid, and 0.05 M MES. The data were fitted by nonlinear regression in Leonora.

Pyruvate α-proton exchange was determined by measuring the loss of pyruvate methyl protons signal in deuterated buffer by ^{1}H NMR (8). Proton exchange assays were performed using 600 μl of assay solution containing 30 mM of pyruvate, 1.0 mM $MgCl_2$ in 20 mM deutered MOPS buffer, pD 8.0.

TABLE 1
HMG aldolase data collection and refinement statistics
The numbers in parentheses indicate the highest resolution shell (1.85 to 1.82).

Data collection	
Space group	R32
Unit cell dimensions	
$a = b$ (Å)	111.18
c (Å)	139.27
Wavelength (Å)	1.541
Resolution limits (Å)	50–1.82
R_{sym}	0.099 (0.273)
Total observations	180,118
Unique observations	27,093
Data completeness (%)	90.8 (89.4)
Redundancy	6.7 (2.8)
$I/\sigma I$	12.0 (4.4)
Mean B (Wilson plot)	28.5
Model refinement	
R_{cryst}	0.158
R_{free}	0.169
Root mean square deviations	
Bond lengths (Å)	0.009
Bond angles (°)	1.20
Residues modeled	2–236
Water molecules	125
Mean B: protein	34.4
Water	46.8
Mg^{2+}	24.4
Pyruvate	26.1
PEG	73.5

RESULTS

Expression and Purification—The HMG/CHA aldolase of *P. putida* F1 was overexpressed in *E. coli* BL21(λDE3) and purified to homogeneity with a typical yield of 19 mg of purified protein/liter of bacterial culture (supplemental Fig. S1 and supplemental Table S1). The subunit molecular mass of the enzyme as determined by SDS-PAGE is 26 kDa, consistent with the predicted molecular mass (25,448 Da).

Overall Structure—The structure of HMG/CHA aldolase was determined at 1.82 Å by molecular replacement using the structure of RraA (Protein Data Bank code 1NXJ) as a search model (Table 1). The protomer forms a four-layered α-β-β-α sandwich (Fig. 2*A*). One layer is a continuous seven-stranded sheet comprised of $\underline{\beta 11'}$, $\underline{\beta 1}$, $\underline{\beta 6}$, $\beta 2$, $\beta 3$, $\beta 4$, and $\beta 5$ (where the underlined strands are antiparallel to others, and $\beta 11'$ is contributed by an adjacent protomer in the trimer). The other β-strand layer is comprised of $\beta 2$, $\underline{\beta 9}$, and $\beta 10$ and, separately, $\beta 7$ and $\underline{\beta 8}$. αC, αD, and αE pack against the exposed face of the first sheet, whereas αA, αB, and the N-terminal portion of αF pack against the exposed face of the second sheet. The C-terminal-most 40 residues form an extended "tail" that wraps around an adjacent protomer of the trimer, with αF, αG, and αH packing against the symmetry related copies of αC and αD and $\beta 11'$ hydrogen bonding with $\beta 1$. The short 3_{10}I helix, found at the very C terminus of the chain, is formed by residues that exist only in the *P. putida* protein.

Oligomeric State—The crystal packs with a single molecule per asymmetric unit. This protomer is associated into a highly stabilized trimer, where each protomer buries 1724 Å^2 with the adjacent protomer; much of this interface is due to the C-terminal extension. PISA calculates that this trimer is the most stable conformation (26). However, there is also a second candidate oligomeric interface where two trimeric rings interact, with a combined 760 Å^2 buried per protomer with two protomers from the opposite ring (Fig. 2, *B* and *C*). Despite this

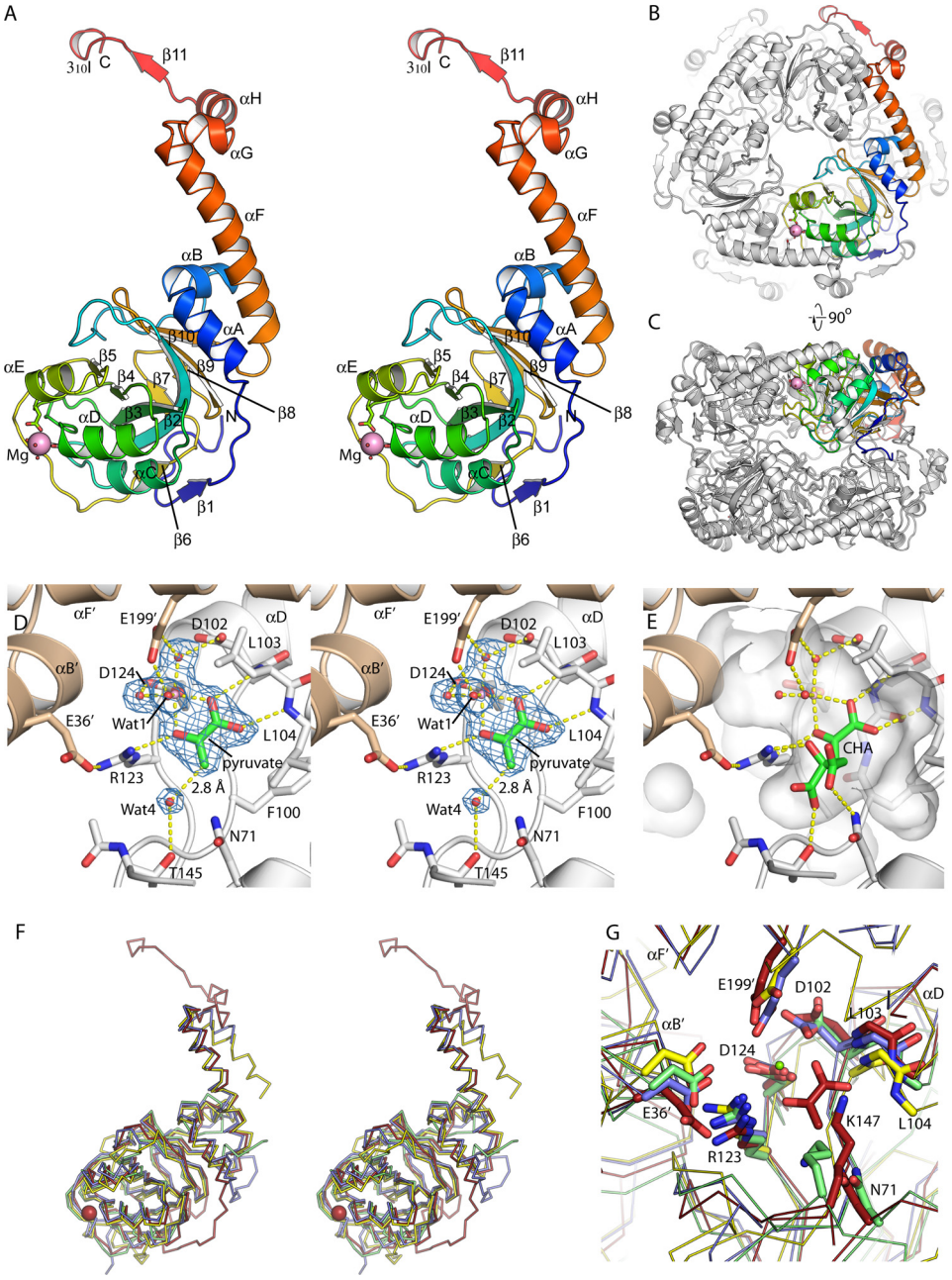

FIGURE 2. **Overall structure of HMG/CHA aldolase.** *A*, organization of the protomer. A single protomer is colored *blue* to *red*, N terminus to C terminus. The magnesium ion is shown as a *magenta sphere*, along with its ligands. Secondary structure elements are labeled. *B*, view of the hexamer, seen down the 3-fold axis. One protomer is colored as in *A*, and the others are in *white*. The C-terminal motif comprising αF, αG, αH, β11, and 3_{10}I wrap around the adjacent protomer, forming extensive interactions. *C*, the hexamer looking down the 2-fold symmetry axis. *D*, active site of HMG/CHA aldolase. One protomer is colored *white*, and the other is *beige*. Electron density for magnesium, pyruvate, and four functionally relevant waters are shown as *blue mesh* at 1.5 σ. *E*, model of CHA in the HMG/CHA aldolase binding in the substrate binding pocket (semitransparent *white surface*). The pyruvate moiety is superposed closely on the experimental pyruvate site. The OH group makes a pair of hydrogen bonds with Wat-1 (the proposed catalytic base) and Arg-123. The carboxylate groups make one direct hydrogen bond each to the protein, with good geometry, as well as to structured water molecules (not shown). *F*, overlay of HMG/CHA aldolase with its homologs. HMG/CHA aldolase is in *red*, 3K4I is in *blue*, 2C5Q is in *yellow*, and RraA (2PCN) is in *green*. Note that HMG/CHA aldolase has N- and C-terminal extensions relative to the other proteins, and 2C5Q has a topological inversion relative to the other structures. *G*, overlay of the catalytic site of HMG/CHA aldolase with its homologs. Structures are colored as in Fig. 2*F*, residues are labeled by their HMG/CHA aldolase convention. Note that the core catalytic machinery associated with pyruvate binding and activation appears conserved across this whole family.

limited buried surface, there are additional lines of evidence indicating that the hexamer is the true, *in vivo* state. The ring-ring interaction shows good shape complementarity, there is a well defined inter-ring hydrophobic patch in the vicinity of Ile-158, and the residues buried at the interface are far more conserved than those on exposed surfaces of the protomer. This proposed hexamer is consistent with a 146-kDa molecular mass determined experimentally by gel filtration.

Active Site Organization—The catalytic site is found in the cleft between adjacent protomers of the trimer and is comprised of residues contributed by helices αD, αE, the β4–αE and β5–β6 loops from one protomer, and αB and αF of the other. The electron density map shows a well ordered magnesium ion and pyruvate molecule bound in the active site (Fig. 2*D*). The magnesium ion displays skewed octahedral coordination geometry. Unusually, the metal ion has only a single direct protein ligand: Asp-124. Two additional coordination sites are occupied by pyruvate, and the remaining three sites are occupied by water molecules. These water molecules are tightly bound, however; one forms a hydrogen bond to Asp-124 carboxylate, one forms a hydrogen bond to the carboxylate groups of Asp-102 and Glu-199′, and the third forms a hydrogen bond to Glu-199′ alone, which is contributed by αF from an adjacent protomer that covers the catalytic site. This helix is stabilized at its N- and C-terminal ends by hydrophobic interactions, but the central two turns are suspended over the catalytic site and solvent-exposed on all sides.

The pyruvate group coordinates the magnesium ion through its keto and one carboxylate oxygen atoms. The pyruvyl carboxylate group also forms a pair of hydrogen bonds with the main chain amide nitrogen atoms of Leu-103 and Leu-104, located at the N-terminal end of αD, whose helix dipole points into the catalytic site. The carbonyl oxygen of pyruvate forms an additional hydrogen bond with the Nε guanadinium nitrogen of Arg-123. Arg-123, in turn, makes a salt bridge with Glu-36. The flat face of the pyruvate stacks against the main chain atoms of Phe-100 and Gly-101. An additional well ordered water molecule (Wat-4)

makes a hydrogen bond (2.8 Å) with the pyruvate methyl group. The ability of the methyl group to act as a hydrogen bond donor reflects the strongly electronegative nature of this methyl carbon atom in the context of the pyruvate·Mg^{2+} complex.

Substrate Modeling—Superposing the pyruvyl moiety of CHA on the experimentally observed pyruvate-binding site allows the rest of the CHA to be modeled by adjusting primarily three torsion angles (Fig. 2*E*). In our model, the C4-OH interacts with Arg-123Nη2 and the metal ligating water molecule, Wat-1, which in turn hydrogen bonds with Glu-199′. The C4-carboxylate hydrogen bonds with Thr-145Oγ. These interactions would all be expected to be recapitulated in the HMG complex. The C6-carboxylate specific to CHA makes a hydrogen bond with Asn-71Nδ and could potentially also hydrogen bond with Lys-147 Nζ, although this would require a slight reorientation of this residue. All of the amino acid residues modeled as contacting the substrate are conserved in all homologous HMG/CHA aldolases (supplemental Fig. S3).

Structurally Related Proteins—Searching the Protein Data Bank with DALI-lite reveals a number of related structures (Fig. 2, *F* and G, and supplemental Table S2). There are two relatively close structural homologs to HMG/CHA aldolase that are functionally uncharacterized: PSPTO_3204 (Protein Data Bank code 3K4I) from *Pseudomonas syringae* pv. tomato DC3000 and YER010c (Protein Data Bank code 2C5Q) from *Saccharomyces cerevisiae* (11). The closest related protein with an established function is the RNaseE inhibitor RraA from *E. coli* (Protein Data Bank code 1Q5X) (10), along with its homologs from *M. tuberculosis* (Protein Data Bank code 1NXJ) (27), *Pseudomonas aeruginosa* (Protein Data Bank code 3C8O), *Thermus thermophilus* (Protein Data Bank code 1J3L) (28), and *Vibrio cholerae* (Protein Data Bank code 1VI4). These RraA homologs omit the first 30 and last 40 amino acids (the C-terminal tail) of HMG/CHA aldolase and are therefore noticeably smaller. The HMG/CHA aldolase structure is also distantly related to His domain of enzyme I for bacterial P-enolpyruvate-dependent carbohydrate:phosphotransferase systems (Protein Data Bank codes 1ZYM and 2HWG) (29, 30) and the phosphotransfer domain of pyruvate phosphate dikinase (Protein Data Bank code 1DIK) (31).

Metal Ion and Substrate Specificity of HMG/CHA Aldolase—The specific activities of purified apoenzyme with different metal ions were determined using HMG as substrate. Optimum activity was obtained with Mg^{2+} and Mn^{2+} ions, and other divalent cations activate the enzyme in the following order of effectiveness: $Co^{2+} > Zn^{2+} > Ni^{2+} > Cd^{2+}$. No detectable activity was observed for Cu^{2+} and Ca^{2+} (Table 2).

Using Mg^{2+} or Mn^{2+} as cofactors, the substrate specificity of HMG/CHA aldolase toward different 4-hydroxy-2-ketoacids was determined (Table 3). The enzyme has the highest specificity constant (k_{cat}/K_m) for CHA and HMG. The specificity constant for HOPA, a substrate analog that lacks the 4-carboxylate group, is decreased by a factor of $\sim 10^4$-fold relative to the physiological substrate, HMG. The enzyme also exhibits oxaloacetate decarboxylase activity, which also involves C–C bond cleavage, leading to formation of pyruvate and carbon dioxide. The kinetic data for all substrates obey classic Michaelis-Menten kinetics except for OAA, which follows a substrate inhibition model.

Pyruvate Proton Exchange and Aldolase pH Rate Profile—The enzyme is able to catalyze the exchange of pyruvate α-proton with a rate of 2.98 ± 0.18 s^{-1} as determined by ^1H NMR in deuterated buffer. Furthermore, sodium oxalate is a strong competitive inhibitor of the HMG aldolase activity with a K_i value of 5.0 ± 0.3 μM using 1.0 mM $MgCl_2$ as a cofactor (supplemental Fig. S2*A*) and 1.7 ± 0.1 μM using 1.0 mM $MnCl_2$ as a cofactor (supplemental Fig. S2*B*).

A pH activity profile for HMG cleavage was determined using constant ionic strength buffers from pH of 6.0 to 10.5, with 1.0 mM $MgCl_2$ as cofactor (supplemental Fig. S4). Kinetic parameters were not determined above pH 10.5 because of the instability of substrate at high pH. The k_{cat}/K_m and k_{cat} data for the enzyme is consistent with a single deprotonation with pK_a values of 8.0 ± 0.1 and 7.0 ± 0.1 for free enzyme and enzyme substrate complex, respectively.

Characterization of the R123A and R123K Variants—Arg-123 was separately replaced with alanine and lysine by site-

TABLE 2

Relative activity of HMG/CHA aldolase with various metal ions

Activity obtained with $MgCl_2$ (0.11 mmol·mg^{-1}·min^{-1}) is taken as 100%. Assays, with the exception of Zn^{2+} and Cu^{2+}, were performed with 2.2 μg of aldolase, 10 mM HMG, 1.0 mM of the respective metal chloride salts, 0.3 mM NADH, 30 units of LDH, and 100 mM sodium HEPES buffer, pH 8.0, in a total volume of 1 ml. Activity with Zn^{2+} and Cu^{2+} was determined by the discontinuous method (8). For assays with Zn^{2+}, a high spontaneous aldol cleavage rate in the presence of 1.0 mM $ZnCl_2$ necessitates that 0.1 mM $ZnCl_2$ be used instead. ND, no activity was detected above the detection limit of 10 nmol·min^{-1}·mg^{-1} protein.

Metal ion	Relative activity
	%
Mg^{2+}	100.0 ± 2.8
Mn^{2+}	90.3 ± 5.7
Co^{2+}	64.7 ± 3.6
Ni^{2+}	28.2 ± 3.4
Cd^{2+}	5.0 ± 0.2
Zn^{2+}	49.6 ± 2.7
Cu^{2+}	ND
Ca^{2+}	ND
EDTA	ND

TABLE 3

Steady state kinetic parameters of HMG/CHA aldolase with different substrates

K_{si} is the substrate inhibition constant.

Substrate	1.0 mM Mg^{2+}				1.0 mM Mn^{2+}			
	K_m	K_{si}	k_{cat}	k_{cat}/K_m	K_m	K_{si}	k_{cat}	k_{cat}/K_m
	mM	mM	s^{-1}	M^{-1}·s^{-1}	mM	mM	s^{-1}	M^{-1}·s^{-1}
OAA	0.30 ± 0.03	0.37 ± 0.04	1.85 ± 0.18	6.2×10^3	0.036 ± 0.004	0.25 ± 0.03	1.52 ± 0.09	4.2×10^4
HMG	0.26 ± 0.02	[a]	19.3 ± 0.9	7.4×10^4	0.022 ± 0.001	[a]	13.7 ± 0.2	6.2×10^5
CHA	0.066 ± 0.008	[a]	14.4 ± 0.5	2.2×10^5	0.030 ± 0.005	[a]	7.5 ± 0.3	2.5×10^5
KHG	0.15 ± 0.02	[a]	0.058 ± 0.002	3.8×10^2	0.071 ± 0.003	[a]	0.25 ± 0.003	3.5×10^3
HOPA	25.0 ± 2.2	[a]	0.048 ± 0.003	1.9	8.8 ± 0.7	[a]	0.19 ± 0.01	2.2×10^1

[a] Substrate inhibition was not observed.

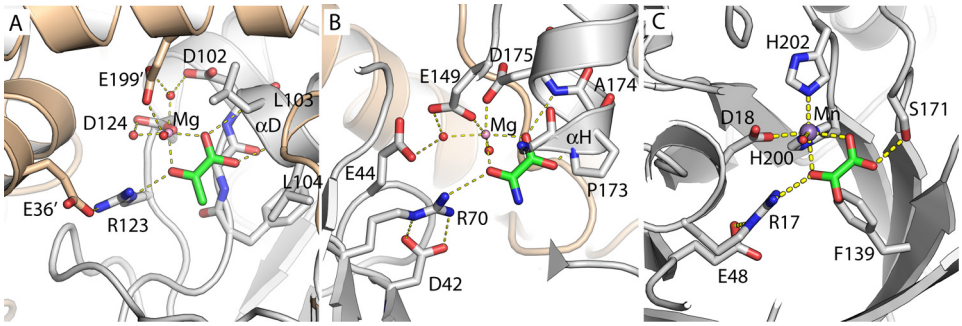

FIGURE 3. **Structural convergence in the active sites of three nonhomologous Class II pyruvate aldolases.** *A*, HMG/CHA aldolase. *B*, HpaI (Protein Data Bank code 2V5K). *C*, DmpG (Protein Data Bank code 1NVM). All three structures are presented from the same perspective, taking the metal ion and pyruvate analog as reference. The residues are labeled. For HpaI, the condensing aldehyde will approach from the distal side of the pyruvate, for DmpG and CHA/HMG aldolase from the proximal side. Note that Arg-123–Glu-36′ pair has a direct analog in both HpaI (Arg-70 to Asp-42) and DmpG (Arg-17 to Glu-48), although the nitrogen atom used to hydrogen bond to the keto oxygen is different in each case. HpaI, like HMG/CHA aldolase, uses a magnesium ion coordinated by acidic groups. The similarities with HpaI extend to the αH region, which acts similarly to αD in HMG/CHA aldolase, providing a pair of hydrogen bonds to the oxamate carboxylate group, as well as a metal ligand (here Asp-175). The peptide bond of Gly-172 to Pro-173 acts similarly to the Phe-100 to Gly-101 peptide bond in HMG/CHA aldolase, packing against the side of pyruvate, albeit against the opposite face. The correspondence with DmpG, which uses a manganese ion, is less apparent. The oxalate carboxylate is coordinated by Ser-171 OH instead of using backbone atoms, and Phe-139 packs against the oxalate rather than the backbone immediately N-terminal to the α-helix.

directed mutagenesis. The R123A mutant proved unable to catalyze pyruvate C3-proton exchange, OAA decarboxylation, and the HMG or CHA aldol cleavage reactions. The R123K variant, on the other hand, retains some HMG aldol cleavage activity (K_m value of 5.5 ± 0.4 mM, k_{cat} value of 0.099 ± 0.001 s^{-1}), although its catalytic efficiency (k_{cat}/K_m) toward HMG is decreased by 4000-fold. This is mainly due to a 200-fold decrease in k_{cat}. Pyruvate proton exchange rate was also reduced by ~200-fold in the R123K variant (0.015 ± 0.003 s^{-1}).

DISCUSSION

Bacterial aromatic *meta*-cleavage pathways follow a general schema wherein a series of steps following aromatic ring cleavage culminates in the formation of a 4-hydroxy-2-ketoacid; this molecule is then cleaved by an aldolase into pyruvate and an aldehyde or ketoacid that is suitable for entry into central metabolism. The HMG/CHA pyruvate aldolase, in particular, catalyzes the last step of protocatechuate 4,5-cleavage pathway. The enzyme adopts a four-layered α-β-β-α sandwich structure with the active site in the interface of two adjacent subunits of the hexamer; this fold has not been previously reported for an aldolase. Two other Class II pyruvate aldolases (HpaI and DmpG) in aromatic *meta*-cleavage pathway (32, 33), along with fructose 1,6-bisphosphate aldolases (34), dihydropteroate synthetases (35), and 3-deoxy-D-manno-octulosonate 8-phosphate synthase (36) all adopt TIM barrel folds. In addition, three-layered α-β-α sandwich structures are reported for L-fuculose-1-phosphate aldolase (37) and rhamnulose-1-phosphate aldolase (38).

In canonical Class II aldolases, the mechanism proceeds via the base-catalyzed abstraction of a proton from the hydroxyl group at the C4 position, cleavage of the carbon-carbon bond, and formation of an enolate intermediate stabilized by a divalent metal ion (39). Protonation of this intermediate forms pyruvate, completing the reaction. The magnesium ion in the HMG/CHA aldolase structure is coordinated directly by Asp-124, and indirectly by Asp-102 and Glu-199′ (from a different protomer), which together position three water molecules that directly bind the metal cofactor. This arrangement most strongly resembles HpaI, where the magnesium ion is bound directly by the acidic residues Glu-149 and Asp-175, whereas Glu-44 is an indirect ligand (Fig. 3*B*) (33). Coordinating this metal ion via the C1-carboxyl and C2-carbonyl groups is a well ordered pyruvate molecule with similar arrangements observed in other pyruvate aldolases containing bound pyruvate analogs (32, 33).

We have shown here that HMG/CHA aldolase catalyzes two reactions: pyruvate C3-proton exchange and oxaloacetate decarboxylation, in addition to HMG and CHA cleavage. All of these reactions require the formation of a pyruvate enolate intermediate. Both HpaI and BphI (56% sequence identity to DmpG) also exhibit pyruvate C3-proton exchange and secondary decarboxylase activity (8, 40), supporting the existence of a common pyruvate enolate intermediate in all three aldolases (5, 7). The presence of this intermediate in these reactions is further supported by oxalate, a pyruvate enolate analog, being a strong competitive inhibitor.

In addition to the pyruvate coordinating metal ion (which characterizes all Class II aldolases), Arg-123 appears to be a functionally critical group. In the pyruvate complex structure it forms a strong hydrogen bond with the pyruvate keto group, and the 200-fold reduction in the α-proton exchange rate in the R123K mutant argues that precise positioning of this hydrogen bond is critical for stabilizing the enolate intermediate. Modeling of the full substrate suggests that this residue also hydrogen bonds to the C4-OH group (Fig. 2*E*). In the C4-OH deprotonation step, Arg-123 is therefore predicted to stabilize the negative charge that develops on the C4-O^-, thus promoting proton abstraction.

Both the k_{cat}/K_m and k_{cat} data indicate a single deprotonation event with pK_a values of 8.0 ± 0.1 and 7.0 ± 0.1 for free enzyme and enzyme substrate complex, respectively. These pK_a values are consistent with a base catalyzed deprotonation of the C4-OH of the substrate leading to the aldol cleavage reaction. The base in this proton abstraction is almost certainly the metal-bound water, Wat-1 (Fig. 4*A*). This group is well positioned to hydrogen bond with C4-OH (2.9 Å), while also interacting with the magnesium ion (which can act as a Lewis acid, stabilizing the hydroxyl ion) and Glu-199′ (which could possibly act in concert with Wat-1 in a proton relay). During the subsequent cleavage of the C3–C4 bond, and the concomitant formation of the enolate intermediate, the hydrogen bond between Arg-123 and the C2 keto oxygen would stabilize the development of a negative charge on this atom (Fig. 4*B*). This critical dual role for Arg-123 is supported by the finding that

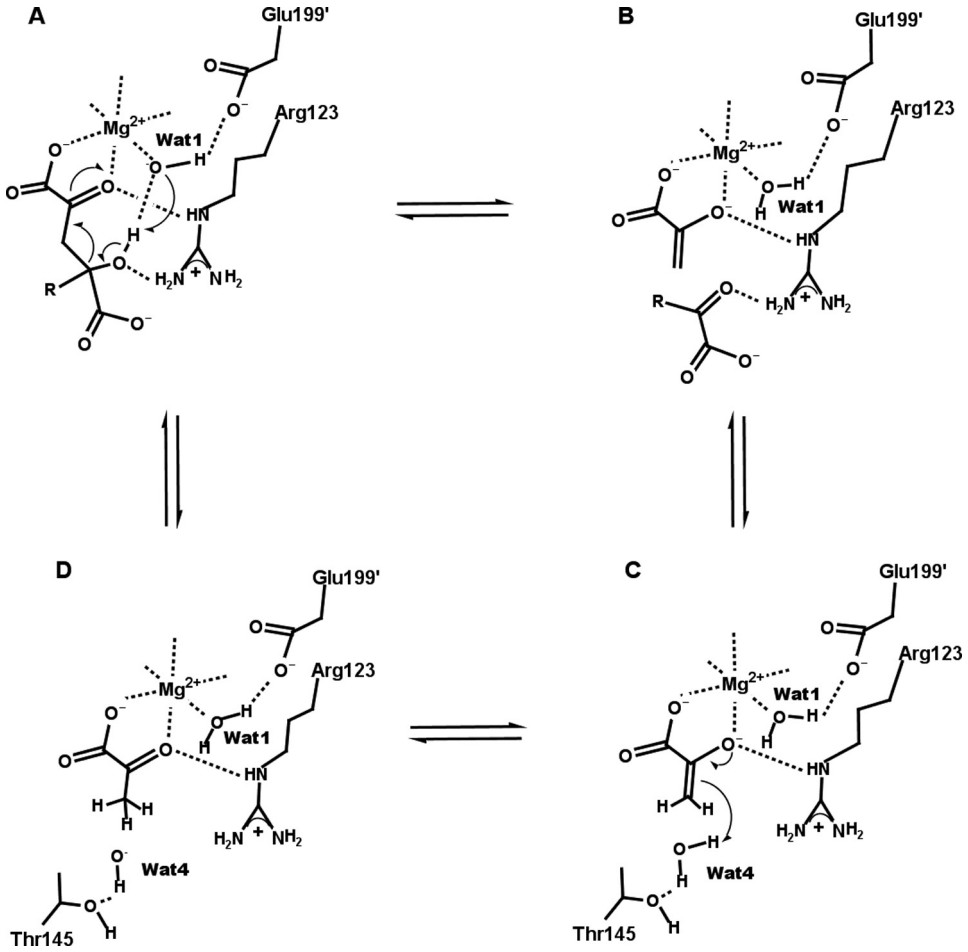

FIGURE 4. **Proposed catalytic mechanism of HMG/CHA aldolase.** *A*, the catalytic cycle starts with substrate binding. A deprotonated metal bound water (Wat-1) abstracts a proton from C4-OH of the substrate. *B*, C–C bond cleavage occurs, pyruvate enolate is formed, and one keto acid product is released. *C*, Wat-4 binds and donates a proton to pyruvate enolate. *D*, pyruvate is formed and can then exchange with a substrate molecule to initiate the next catalytic cycle.

replacement with Lys results in an enzyme with greatly reduced activity (indicating that both H-bond-donating groups are likely needed), whereas replacement with Ala results in a protein that is wholly inactive. The disruption of the pyruvate C3 deuterium exchange and the OAA decarboxylation reactions in addition to HMG cleavage supports the idea that Arg-123 is especially important for stabilizing the enolate anion. Intriguingly, in the active sites of both HpaI and DmpG, an arginine residue is positioned to present a pair of guanylate nitrogen atoms in nearly identical (relative to pyruvate) positions (Fig. 3). In HpaI, replacement of Arg-70 with an alanine residue also abolishes aldolase activity. Together, these common features in HMG/CHA, HpaI, and DmpG aldolases point toward the convergent evolution of a common catalytic mechanism. Other enzymes that also proceed through a metal ion-assisted 2-keto-acid enolization reaction step, such as oxaloacetate decarboxylase (PA4872) (41) and 5,10-methylenetetrahydrofolate:3-methyl-2-oxobutanoate hydroxymethyl transferase (42), also have arginine residues (Arg-159 for PA4872 and Arg-228 for KPHMT from *M. tuberculosis*) interacting with the equivalent substrate keto group in their active sites.

The final step of the cleavage reaction is protonation of the pyruvate enolate, forming pyruvate (Fig. 4*C*). The experimental, pyruvate-bound structure represents the product of this reaction, and Wat-4 (which forms a 2.8 Å hydrogen bond with the methyl hydrogen) is the only observed nearby group capable of proton donation (Fig. 2*D*). Although this water is likely a relatively poor acid (there are no nearby charged residues to stabilize a hydroxide or hydronium ion), the relatively slow nature of this step means that it should still suffice to explain the observed catalytic rate.

Despite the acidic metal ion-binding pocket, the presence of the magnesium ion and multiple cationic residues (Arg-40, Arg-123, Arg-195, Arg-203, Lys-147, and Lys-202) result in the active site being generally electropositive. This likely contributes to the specificity of the enzyme toward substrates with 4-carboxylate substitutions, such as HMG and CHA. Additional interactions of the substrate with conserved residues including Thr-145, Asn-71, and Lys-147 are probably important for the C4–C6 moiety of CHA binding and correctly positioning the substrate. This area may also be a second position for nonproductive OAA binding, accounting for the substrate inhibition kinetics for OAA decarboxylation activity (Table 3). In general, substrate recognition does not appear to involve tight interactions, resulting in the relative broad substrate specificity of the enzyme.

The structural and mechanistic insight afforded by this study also sheds light on several related proteins whose functions are poorly understood. For example, the structure of YER010c, from *S. cerevisiae* was reported, but whereas the hypothesis of it being a methyltransferase was discounted (11), a more plausible function has not been demonstrated. Even more closely related is PSPTO_3204 (Protein Data Bank code 3K4I) from *P. syringae* pv. tomato DC3000, which was recently deposited at the Protein Data Bank but without an ascribed function. Most of the key catalytic machinery identified in HMG/CHA aldolase, including the metal ligands Asp-102 (although not in YER010c), Asp-124, and Glu-199′, the keto binding Arg-123 along with Glu-36, as well as the residues contributed by α_D, have direct correlates in YER010c and PSPTO_3204 (Fig. 2*G* and supplemental Fig. S5). Interestingly, a magnesium ion in the PSPTO_3204 structure is ligated directly to Asp-102 and Glu-200 and indirectly to Asp-124. This position is shifted ~3 Å relative to HMG/CHA aldolase and appears incompatible with productive pyruvate binding. In both of these enzymes, a deep binding pocket is present, but loop rearrangements and

residue replacements result in the binding sites being quite different, suggesting the recognition of quite different substrates. Nevertheless, the strong conservation of the magnesium and pyruvate-binding sites in these two proteins argues that they too are highly likely to be aldolases.

The similarity between HMG/CHA aldolase and RraA is less strong. RraA from *E. coli* is proposed to bind the C-terminal domain of RNase E, blocking binding of accessory proteins involved in the RNA degradosome function (43, 44). RraA is also trimeric but, relative to HMG/CHA aldolase, lacks several motifs (supplemental Fig. S5), including the αF helix that contributes the metal ligand Glu-199′. The equivalent of Arg-123 is conserved across all RraA homologs, whereas Asp-102 and Asp-124 are also largely conserved, although one or both are missing in some homologs, including *E. coli* and *T. thermophilus*. Interestingly, the proposed substrate-binding residues Asn-71 and Lys-147 are conserved, despite RraA being relatively distantly related to HMG/CHA aldolase. The pyruvate-binding site is occupied by small anions in several of these structures, including tartaric acid (Protein Data Bank code 1NXJ) and acetate (Protein Data Bank code 2PCN). RraA is present in organisms such as *T. thermophilus* (28) where RNase E is absent, suggesting that the inhibitory function of RraA may have been secondarily acquired, and some homologs may have a catalytic function in addition to, or instead of, the RNase E inhibitory function. The similarities with the active site of HMG/CHA aldolase suggests that the RraA family is derived from a common ancestor with class II aldolase activity, and at least some homologs seem likely to have retained this activity. In addition, HMG/CHA aldolase is also distantly related to the His domain of Enzyme I and phosphohistidine domain of PPDK in terms of the three-dimensional structure. Intriguingly, the histidine residues responsible for phosphate transfer (His-189 for enzyme I and His-455 for PPDK) were replaced by arginine (Arg-123) in HMG/CHA aldolase, which is essential for catalysis. Future work on these proteins may provide deeper insights into how these divergent functions evolved from a common ancestor.

Acknowledgment—We thank Pawel Grochulski for collecting the HMG/CHA aldolase dataset at the Canadian Macromolecular Crystallography Facility.

REFERENCES

1. Masai, E., Katayama, Y., and Fukuda, M. (2007) *Biosci. Biotechnol. Biochem.* **71,** 1–15
2. Seo, J. S., Keum, Y. S., and Li, Q. X. (2009) *Int. J. Environ. Res. Public Health* **6,** 278–309
3. Keyser, P., Pujar, B. G., Eaton, R. W., and Ribbons, D. W. (1976) *Environ. Health Perspect.* **18,** 159–166
4. Dennis, D. A., Chapman, P. J., and Dagley, S. (1973) *J. Bacteriol.* **113,** 521–523
5. Tack, B. F., Chapman, P. J., and Dagley, S. (1972) *J. Biol. Chem.* **247,** 6444–6449
6. Maruyama, K. (1990) *J. Biochem.* **108,** 327–333
7. Maruyama, K., Miwa, M., Tsujii, N., Nagai, T., Tomita, N., Harada, T., Sobajima, H., and Sugisaki, H. (2001) *Biosci. Biotechnol. Biochem.* **65,** 2701–2709
8. Wang, W., and Seah, S. Y. (2005) *Biochemistry* **44,** 9447–9455
9. Powlowski, J., Sahlman, L., and Shingler, V. (1993) *J. Bacteriol.* **175,** 377–385
10. Monzingo, A. F., Gao, J., Qiu, J., Georgiou, G., and Robertus, J. D. (2003) *J. Mol. Biol.* **332,** 1015–1024
11. Leulliot, N., Quevillon-Cheruel, S., Graille, M., Schiltz, M., Blondeau, K., Janin, J., and Van Tilbeurgh, H. (2005) *Protein Sci.* **14,** 2751–2758
12. Clapés, P., Fessner, W. D., Sprenger, G. A., and Samland, A. K. (2010) *Curr. Opin. Chem. Biol.* **14,** 154–167
13. Sambrook, J., Fritsch, E. F., and Maniatis, T. (1989) *Molecular Cloning: A Laboratory Manual*, Cold Spring Harbor Laboratory, Cold Spring Harbor, New York
14. Tabor, S., and Richardson, C. C. (1985) *Proc. Natl. Acad. Sci. U.S.A.* **82,** 1074–1078
15. Bradford, M. M. (1976) *Anal. Biochem.* **72,** 248–254
16. Otwinowski, Z., and Minor, W. (1997) *Methods Enzymol.* **276,** 307–326
17. McCoy, A. J., Grosse-Kunstleve, R. W., Adams, P. D., Winn, M. D., Storoni, L. C., and Read, R. J. (2007) *J. Appl. Crystallogr.* **40,** 658–674
18. Emsley, P., Lohkamp, B., Scott, W. G., and Cowtan, K. (2010) *Acta Crystallogr. D Biol. Crystallogr.* **66,** 486–501
19. Collaborative Computational Project (1994) *Acta Crystallogr. D Biol. Crystallogr.* **50,** 760–763
20. Winn, M. D., Isupov, M. N., and Murshudov, G. N. (2001) *Acta Crystallogr. D Biol. Crystallogr.* **57,** 122–133
21. Delano, W. L. (2002) *The PyMOL Molecular Graphics System*, DeLano Scientific, San Carlos, CA
22. Helaine, V., Rossi, J., Gefflaut, T., Alaux, S., and Bolte, J. (2001) *Adv. Synth. Catalysis* **343,** 692–697
23. Wang, W., Baker, P., and Seah, S. Y. (2010) *Biochemistry* **49,** 3774–3782
24. Chell, R. M., Sundaram, T. K., and Wilkinson, A. E. (1978) *Biochem. J.* **173,** 165–177
25. Cornish-Bowden, A. (1995) *Analysis of Enzyme Kinetic Data*, Oxford University Press, New York
26. Krissinel, E., and Henrick, K. (2007) *J. Mol. Biol.* **372,** 774–797
27. Johnston, J. M., Arcus, V. L., Morton, C. J., Parker, M. W., and Baker, E. N. (2003) *J. Bacteriol.* **185,** 4057–4065
28. Rehse, P. H., Kuroishi, C., and Tahirov, T. H. (2004) *Acta Crystallogr. D Biol. Crystallogr.* **60,** 1997–2002
29. Liao, D. I., Silverton, E., Seok, Y. J., Lee, B. R., Peterkofsky, A., and Davies, D. R. (1996) *Structure* **4,** 861–872
30. Teplyakov, A., Lim, K., Zhu, P. P., Kapadia, G., Chen, C. C., Schwartz, J., Howard, A., Reddy, P. T., Peterkofsky, A., and Herzberg, O. (2006) *Proc. Natl. Acad. Sci. U.S.A.* **103,** 16218–16223
31. Herzberg, O., Chen, C. C., Kapadia, G., McGuire, M., Carroll, L. J., Noh, S. J., and Dunaway-Mariano, D. (1996) *Proc. Natl. Acad. Sci. U.S.A.* **93,** 2652–2657
32. Manjasetty, B. A., Powlowski, J., and Vrielink, A. (2003) *Proc. Natl. Acad. Sci. U.S.A.* **100,** 6992–6997
33. Rea, D., Fülöp, V., Bugg, T. D., and Roper, D. I. (2007) *J. Mol. Biol.* **373,** 866–876
34. Blom, N. S., Tétreault, S., Coulombe, R., and Sygusch, J. (1996) *Nat. Struct. Biol.* **3,** 856–862
35. Hampele, I. C., D'Arcy, A., Dale, G. E., Kostrewa, D., Nielsen, J., Oefner, C., Page, M. G., Schönfeld, H. J., Stüber, D., and Then, R. L. (1997) *J. Mol. Biol.* **268,** 21–30
36. Radaev, S., Dastidar, P., Patel, M., Woodard, R. W., and Gatti, D. L. (2000) *J. Biol. Chem.* **275,** 9476–9484
37. Dreyer, M. K., and Schulz, G. E. (1993) *J. Mol. Biol.* **231,** 549–553
38. Kroemer, M., Merkel, I., and Schulz, G. E. (2003) *Biochemistry* **42,** 10560–10568
39. Horecker, B. L., Tsolas, O., and Lai, C. Y. (1972) in *The Enzymes* (Boyer, P. D., ed) 3rd Ed., Vol. 7, pp. 213–258, Academic Press, New York
40. Baker, P., Pan, D., Carere, J., Rossi, A., Wang, W., and Seah, S. Y. (2009) *Biochemistry* **48,** 6551–6558
41. Narayanan, B. C., Niu, W., Han, Y., Zou, J., Mariano, P. S., Dunaway-Mariano, D., and Herzberg, O. (2008) *Biochemistry* **47,** 167–182
42. Chaudhuri, B. N., Sawaya, M. R., Kim, C. Y., Waldo, G. S., Park, M. S., Terwilliger, T. C., and Yeates, T. O. (2003) *Structure* **11,** 753–764
43. Górna, M. W., Pietras, Z., Tsai, Y. C., Callaghan, A. J., Hernández, H., Robinson, C. V., and Luisi, B. F. (2010) *RNA* **16,** 553–562
44. Lee, K., Zhan, X., Gao, J., Qiu, J., Feng, Y., Meganathan, R., Cohen, S. N., and Georgiou, G. (2003) *Cell* **114,** 623–634